Steady-State Multiplicity in a Solid Oxide Fuel Cell

Mona Bavarian and Masoud Soroush

Abstract— Steady-state multiplicity in a solid oxide fuel cell (SOFC) in constant ohmic external load, potentiostatic, and galvanostatic operation modes is studied using a detailed first-principles lumped model. The SOFC model is derived by accounting for heat and mass transfer as well as electrochemical processes taking place inside the fuel cell. Conditions under which the fuel cell exhibits steady-state multiplicity are determined. The effects of operating conditions such as the convection heat transfer coefficient, and the inlet fuel and air temperatures and velocities on the steady state multiplicity regions are studied. Depending on the operating conditions, the cell exhibits one or three steady states. For example, it has three steady states at low external load resistances in the constant ohmic external load mode, and at low cell voltages in the potentiostatic mode.

I. INTRODUCTION

Fuel cells have attracted a lot of attentions in the past two decades because of the worldwide need for more efficient and greener power generation systems. Among various fuel cell types, solid oxide fuel cells (SOFCs) have several advantages, including higher fuel flexibility, need for less expensive catalysts, and more resistance to catalyst poisoning [1]. Typically, SOFCs operate in a high temperature range of 600-1000°C [2].

There have been two previous theoretical studies [3, 4] pointing to the presence of multiple steady states in SOFCs. As no experimental evidence has been reported yet, can a true (realistic) SOFC exhibit steady-state multiplicity? Our first attempt to answer this question is to depart from the simple lumped models considered in [3, 4] and study the steady-state behavior of a more realistic lumped model of a SOFC.

Steady-state multiplicity reported for SOFCs in [3, 4] arises as a consequence of exponential increase in the electrolyte (zirconia) ionic conductivity with electrolyte temperature. An increase in solid (electrolyte) temperature reduces the electrolyte resistance with respect to oxygen anion transport, which in turn increases the current drawn from the cell and accordingly increases the rate of the exothermic reactions occurring at the electrolyte interface and therefore the electrolyte temperature. Thus, the positive feedback between oxygen anion migration and the electrolyte temperature is responsible for the steady state multiplicity in SOFCs.

Thermal management in SOFCs is very important. Temperature control is needed to prevent degradation of the fuel cells at high temperatures, and maintain a high efficiency because of the dependence of the electrolyte conductivity on temperature. The existence of the multiplicity in SOFCs can make temperature control of the fuel cells as well as the auxiliary components in the fuel cell systems more challenging and can limit the performance of the fuel cell controllers.

This paper presents a bifurcation study of a SOFC using a fuel cell model that is more realistic than the two lumped models considered in the previous studies [3, 4]. An objective is to investigate the effects of cell parameter values on steady-state multiplicity and the location of steady states. A more detailed mathematical model is first developed. Heat transfer, mass transfer and electrochemical processes are taken into account. Three different operation modes, under constant ohmic external load, potentiostatic control and galvanostatic control, are studied. The existence of a unique steady state or multiple steady states in the cell is investigated in terms of the cell inlet air and fuel temperatures and velocities, the convection heat transfer coefficient, and the ohmic external load. The ranges of operating conditions for which steady state multiplicity exists are determined.

The remainder of this article is organized as follows. Section II describes the mathematical model of the SOFC. Section III presents the steady-state analysis results. Concluding remarks are presented in Section IV.

II. MATHEMATICAL MODELING

The SOFC system under study is a single planar SOFC. Figure 1 shows the schematic of the SOFC. A model is developed using the approach presented in [5]. Here, the fuel cell was divided into five subsystems: 1) a solid part which consists of the anode, cathode and electrolyte layers, 2) the diffusion layer inside the cathode side, 3) the gas channel on the cathode side, 4) the diffusion layer inside the anode side, and 5) the gas channel on the anode side. The following assumptions are made:

   (i) Each subsystem is locally homogeneous; each subsystem is considered as a stirred tank.

   (ii) Heat transfer coefficients for convection between the anode and the fuel stream and between the cathode and the air stream are constant.

   (iii) Heat transfer by radiation between the electrodes and the gases in the anode and cathode side channels is ignored.

M. Bavarian and M. Soroush are with the Department of Chemical and Biological Engineering, Drexel University, Philadelphia, PA 19104, USA.
Corresponding author: M. Soroush, ms1@drexel.edu

(iv) All gases are ideal.

A. *Electrochemical Modeling*

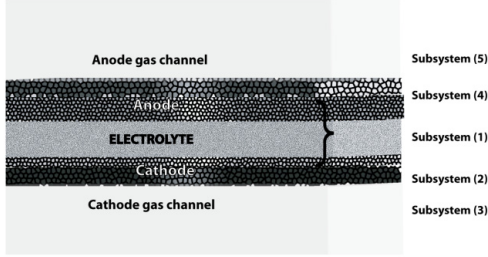Electrochemical reactions taking place inside a SOFC when hydrogen is used as a fuel are [6] :
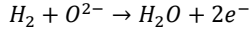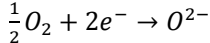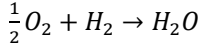

Fig. 1. Planar SOFC divided into five subsystems.

Oxidation reaction at the anode side:

$$H_2 + O^{2-} \rightarrow H_2O + 2e^-$$

Reduction reaction at the cathode side:

$$\frac{1}{2}O_2 + 2e^- \rightarrow O^{2-}$$

So, the overall reaction is:

$$\frac{1}{2}O_2 + H_2 \rightarrow H_2O$$

Rates of hydrogen consumption, oxygen consumption and water production are directly calculated from the cell current using Faraday's law:

$$R_{H_2} = \left(\frac{1}{2F}\right)I \tag{1}$$

$$R_{O_2} = \left(\frac{1}{4F}\right)I \tag{2}$$

$$R_{H_2O} = \left(\frac{1}{2F}\right)I \tag{3}$$

The reversible cell voltage is calculated using the Nernst equation:

$$U^0 = E^0 - \frac{RT^S}{2F}ln(\frac{p_{H_2O}^{bulk}}{p_{H_2}^{bulk}p_{O_2}^{bulk\,0.5}})) \tag{4}$$

The actual cell output voltage is lower than the reversible voltage calculated using the Nernst equation because of three potential drops/losses: ohmic polarization, concentration polarization, and activation polarizations. Subtracting these losses from the reversible cell voltage yields the cell outlet voltage:

$$U^{cell} = U^0 - \eta^A - \eta^C - \rho^E d^E i - \eta_{conc} \tag{5}$$

where η^A and η^C represent the anode and cathode activation polarizations, respectively. These polarizations are described by Butler-Volmer equation for the anode and cathode sides [4]:

$$\frac{I}{LB} = \gamma^A p_{H_2}^{TPB} p_{H_2O}^{TPB} \, exp\left(\frac{-E^A}{RT^s}\right)\left\{exp\left(\theta_a^A \frac{F}{RT^s}\eta^A\right)\right.$$
$$\left. - exp\left(-\theta_c^A \frac{F}{RT^s}\eta^A\right)\right\} \tag{6}$$

$$\frac{I}{LB} = \gamma^A p_{O_2}^{TPB\,0.25} \, exp\left(\frac{-E^C}{RT^s}\right)\left\{exp\left(\theta_a^C \frac{F}{RT^s}\eta^C\right)\right.$$
$$\left. - exp\left(-\theta_c^C \frac{F}{RT^s}\eta^C\right)\right\} \tag{7}$$

The activation overvoltages (polarizations) represent the voltage needed to overcome the activation energies of electrochemical reactions occurring in the triple phase boundary (TPB) [11].

The fourth term in the right hand side of the Eq.(5), $\rho^E d^E i$, accounts for ohmic losses. Ohmic losses are mainly due to ionic resistance of electrolyte rather than the electrical resistance in the electrodes. Electrical resistivity of the electrolyte is described by an Arrhenius type correlation, dependent on temperature [7]:

$$\rho^E = \frac{1}{\beta_1}\exp\left(\frac{\beta_2}{T^S}\right) \tag{8}$$

To account for the concentration polarization, the following correlation is used [12]:

$$\eta_{conc} = \frac{RT}{nF}ln(\frac{p_{H_2O}^{TPB}}{p_{H_2}^{TPB} \, p_{O_2}^{TPB\,0.5}}) - \frac{RT}{nF}ln(\frac{p_{H_2O}^{bulk}}{p_{H_2}^{bulk} \, p_{O_2}^{bulk\,0.5}}) \tag{9}$$

which is indeed the difference between two reversible cell voltages, one calculated based on bulk partial pressures of species and the other calculated based on the partial pressures of species at the triple phase boundary.

For each of the five subsystems, mass and energy conservation equations are written, leading to fourteen (ten ordinary differential and four algebraic) nonlinear equations.

B. *Model Equations for Subsystem 1*

Subsystem 1 is the solid phase of the cell, which consists of the anode layer, the cathode layer, and the electrolyte layer between them. Heat is transferred between the solid and gas streams in the anode and cathode gas channels by convection heat transfer. Heat generated in the cell is the difference between the energy released by the electrochemical reaction and the electric power supplied to the external load. An energy balance for this subsystems yields:

$$(d_A + d_E + d_C)(\rho c_p)^s \frac{dT^s}{dt} = \Delta H_R - \left((\phi^C - \phi^A)I\right)\frac{1}{LB} + \alpha(T_{fuel}^{an} - T^S) + \alpha(T_{air}^{cat} - T^S) \tag{10}$$

where

$$\Delta H_R = N_{O_2}H_{O_2}^{cat} + N_{H_2}H_{H_2}^{an} - N_{H_2O}H_{H_2O}^{an}$$

C. *Model Equations for Subsystem 2*

This subsystem embodies the diffusion layer in the cathode side of the fuel cell. A mole balance on the oxygen inside the cathode-side diffusion layer leads to:

$$\frac{\Delta_{cat}}{R}\frac{d}{dt}\left(\frac{p_{O_2}^{TPB}}{T^S}\right) = N_{O_2} - \frac{1}{LB}R_{O_2} \tag{11}$$

where R_{O_2} is the molar rate of consumption of oxygen, described in Section A, and N_{O_2} is the molar flux of oxygen transferred from the cathode side channel into this layer. The mass flux of the diffusing oxygen can be defined in terms of the mass transfer coefficient by

$$N_{O_2} = k_{O_2}^{cat}(c_{air}^{cat}y_{O_2}^{cat} - \frac{p_{O_2}^{TPB}}{RT^S}) \tag{12}$$

where $k_{O_2}^{cat}$ is the mass transfer coefficient, is given by

$$k_{O_2}^{cat} = \frac{D_{eO_2}}{\Delta_{cat}} = \left(\frac{\varepsilon_{cat}}{\tau_{cat}\Delta_{cat}}\right)D_{O_2} \tag{13}$$

$D_{e_{O_2}}$ is the effective diffusion coefficient, ε_{cat} and τ_{cat} are respectively the porosity and tortuosity of the cathode porous materials, Δ_{cat} is the thickness of the cathode diffusion layer, and D_{O_2} is the total diffusion coefficient, which includes Knudsen and molecular combined diffusion given by [10]:

$$\frac{1}{D_{O_2}} = \frac{1}{D_{O_2N_2}} + \frac{1}{D_{K_{O_2}}} \qquad (14)$$

The binary diffusion coefficient of oxygen in nitrogen is calculated using the Fuller correlation:

$$D_{O_2N_2} = \frac{1.013*10^{-7}(T^S)^{1.75}(\frac{1}{M_{O_2}}+\frac{1}{M_{N_2}})^{0.5}}{\left[p_{O_2}^{TPB}+p_{air}^{cat}\left(1-y_{O_2}^{cat}\right)\right][v_{O_2}^{\frac{1}{3}}+v_{N_2}^{\frac{1}{3}}]^2} \qquad (15)$$

For straight and round pores, the Knudsen diffusion coefficient is given by [9]:

$$D_{K_{O_2}} = 97\,\delta_{cat}\sqrt{\frac{T^S}{M_{O_2}}} \qquad (16)$$

D. *Model Equations for Subsystem 3*

This subsystem is the cathode gas channel in which air flows through. The dynamics of this subsystem are described by the following three equations obtained from a mole balance on air, a mole balance on oxygen and an energy balance:

$$(LBH^c)\frac{dc_{air}^{cat}}{dt} = \dot{n}_{air,in}^{cat} - v_{air}^{cat}c_{air}^{cat}H^cB - N_{o_2}(LB) \qquad (17)$$

$$(LBH^c)\frac{d(c_{air}^{cat}y_{o_2}^{cat})}{dt} = \dot{n}_{air,in}^{cat}y_{o_2,in} - v_{air}^{cat}c_{air}^{cat}y_{o_2}^{cat}H^cB - N_{o_2}(LB) \qquad (18)$$

$$(LBH^c)\frac{d(c_{air}^{cat}c_{p_{air}}^{cat}T_{air}^{cat})}{dt} = \dot{n}_{air,in}^{cat}H_{air,in}^{cat} - v_{air}^{cat}c_{air}^{cat}H_{air}^{cat}(BH^c) + \alpha(T^S - T_{air}^{cat})(LB) - N_{o_2}H_{O_2}^{cat}(LB) \qquad (19)$$

The first term from the right in Eq.(19) accounts for energy leaving the subsystem with the oxygen that diffuses into the cathode layer.

E. *Model Equations for Subsystem 4*

This subsystem represents the diffusion layer in the anode side of the fuel cell. The mole balances on the two species present in this layer, hydrogen and water, are as follows:

$$\frac{\Delta_{ano}}{R}\frac{d}{dt}\left(\frac{p_{H_2O}^{TPB}}{T^S}\right) = -N_{H_2O} + \frac{1}{LB}R_{H_2O} \qquad (20)$$

$$\frac{\Delta_{ano}}{R}\frac{d}{dt}\left(\frac{p_{H_2}^{TPB}}{T^S}\right) = N_{H_2} - \frac{1}{LB}R_{H_2} \qquad (21)$$

where R_{H_2} and R_{H_2O} are the molar rates of hydrogen consumption and water production, described in Section A. N_{H_2} and N_{H_2o} are molar fluxes of hydrogen flowing out of and water flowing into this layer. These fluxes are given by:

$$N_{H_2} = k_{H_2}^{an}(c_{fuel}^{an}y_{H_2}^{an} - \frac{p_{H_2}^{TPB}}{R\,T^S}) \qquad (22)$$

$$N_{H_2O} = k_{H_2O}^{an}(\frac{p_{H_2O}^{TPB}}{R\,T^S} - c_{fuel}^{an}y_{H_2O}^{an}) \qquad (23)$$

The mass transfer coefficients of water and hydrogen are given by:

$$k_{H_2}^{an} = \frac{D_{e_{H_2}}}{\Delta_{ano}} = (\frac{\varepsilon_{ano}}{\tau_{ano}\Delta_{ano}})D_{H_2} \qquad (24)$$

$$k_{H_2O}^{an} = \frac{D_{e_{H_2O}}}{\Delta_{ano}} = (\frac{\varepsilon_{ano}}{\tau_{ano}\Delta_{ano}})D_{H_2O} \qquad (25)$$

where ε_{ano} and τ_{ano} are the porosity and tortuosity of the anode porous materials; and D_{H_2} and D_{H_2O} are the total diffusion coefficients of hydrogen and water, calculated from:

$$\frac{1}{D_{H_2}} = \frac{1}{D_{H_2H_2O}} + \frac{1}{D_{K_{H_2}}} \qquad (26)$$

$$\frac{1}{D_{H_2O}} = \frac{1}{D_{H_2OH_2}} + \frac{1}{D_{K_{H_2O}}} \qquad (27)$$

where

$$D_{K_{H_2}} = 97\,\delta_{ano}\sqrt{\frac{T^S}{M_{H_2}}}$$

and

$$D_{K_{H_2O}} = 97\,\delta_{ano}\sqrt{\frac{T^S}{M_{H_2O}}}$$

The binary diffusion coefficient of hydrogen in water, $D_{H_2H_2O}$, is equal to that of water in hydrogen, $D_{H_2OH_2}$, and is calculated using the Fuller equation:

$$D_{H_2H_2O} = \frac{1.013*10^{-7}(T^S)^{1.75}[\frac{1}{M_{H_2}}+\frac{1}{M_{H_2O}}]^{0.5}}{\left(p_{H_2O}^{TPB}+p_{H_2}^{TPB}\right)(v_{H_2}^{\frac{1}{3}}+v_{H_2O}^{\frac{1}{3}})^2} \qquad (28)$$

F. *Model Equations for Subsystem 5*

This subsystem is the anode-side channel gas including hydrogen and water. A total mole balance on the fuel, a mole balance on hydrogen, and an energy balance yield:

$$(LBH^A)\frac{dc_{fuel}^{an}}{dt} = \dot{n}_{fuel,in}^{an} - v_{fuel}^{an}c_{fuel}^{an}H^AB + (N_{H_2O} - N_{H_2})(LB) \qquad (29)$$

$$(LBH^A)\frac{d(c_{fuel}^{an}y_{H_2}^{an})}{dt} = \dot{n}_{fuel,in}^{an}y_{H_2,in} - v_{fuel}^{an}c_{fuel}^{an}y_{H_2}^{an}H^AB - N_{H_2}(LB) \qquad (30)$$

$$(LBH^A)\frac{d(c_{fuel}^{an}c_{p_{fuel}}^{an}T_{fuel}^{an})}{dt} = \dot{n}_{fuel,in}^{an}H_{fuel,in}^{an} - v_{fuel}^{an}c_{fuel}^{an}H_{fuel}^{an}(BH^A) + \alpha(T^S - T_{fuel}^{an})(LB) + (N_{H_2O}H_{H_2O}^{an} - N_{H_2}H_{H_2}^{an})(LB) \qquad (31)$$

III. STEADY STATE ANALYSIS

The model consists of fourteen (ten ordinary differential and four algebraic) equations. At steady state conditions, it reduces to fourteen algebraic equations. For operation under a constant ohmic load, these equations need to be solved to obtain the steady state values of $p_{O_2}^{TPB}$, c_{air}^{cat}, $y_{o_2}^{cat}$, T_{air}^{cat}, $p_{H_2O}^{TPB}$, $p_{H_2}^{TPB}$, c_{fuel}^{an}, $y_{H_2}^{an}$, T_{fuel}^{an}, I, V, η^A, η^C and T^S corresponding to a given value of R_{load}. The model parameter values are listed in Table 1.

In the case of a constant ohmic load, load resistance (R_{load}) is selected as the bifurcation parameter. For a given load resistance (R_{load}), multiple steady-state values may exist for the solid temperature (T^S). Thus, if we set the value of the load resistance, a numerical root-finding method finds the steady-state solid temperature that is closest to the initial guess used. On the other hand, for a given solid temperature (T^S), one load resistance (R_{load}) always exists. Therefore, if we set the value of T^S, rather than R_{load}, one suitable initial guess will be adequate. Furthermore, as the dependence of the cell behavior on the solid temperature is highly

nonlinear, by setting the temperature and solving for the remaining variables one eliminates the most severe nonlinearity from the system of algebraic equations. The MATLAB routine `fsolve` is used to solve the algebraic equations. After a solution is obtained for a fixed value of the solid temperature, for the next fixed value of the solid temperature, the root corresponding to the previous value of the solid temperature is chosen as the initial guess vector. This approach reduces the convergence time and results in less numerical errors.

The number of steady state solutions can be found by calculating and plotting the heat generation and heat removal rates in the cell versus the solid temperature, as in the study of steady-state multiplicity in chemical reactors. The heat generation and heat removal rates are equal at a steady state. The heat removal is by convection heat transfer and increases linearly with the solid temperature, while the heat generation increases sigmoidally. Three modes of operation, under constant external load resistance, potentiostatic control and galvanostatic control, are considered herein.

A. Constant Ohmic Load Operation

Under a constant ohmic load, the ohm's law is used to describe the cell voltage and current relation:

$$\Phi^C - \Phi^A = R_{Load}I$$

To investigate the existence of multiple steady states under constant ohmic load operation, we carry out a bifurcation analysis with equal inlet air and inlet fuel temperatures of 950 K. Figure 2(a) depicts heat generation and heat removal curves versus the solid temperature for an external load resistance of 0.0112 Ω. As can be seen, there are three steady states (steady state temperatures) corresponding to the load level. The middle steady state, as expected, is unstable. The corresponding T^S-R_{Load} plot is shown in Figure 2(b). This figure shows that for a load resistance between 0.0110 to 0.0114 Ω, there are three values for the solid temperature. It also indicates that this system exhibits hysteresis behavior, which involves two-saddle node bifurcations. If the cell external load resistance is in this range, and the load resistance is gradually lowered, the steady state moves toward point A, which is the ignition point. At this point, with a small further decrease in the load resistance, the temperature jumps to point B on the upper branch. As the load is increased at this point, the cell moves towards operating at point C, which is the extinction point. With a small further increase, the temperature drops sharply to the lower curve. Points A and C represent the boundaries of hysteresis loop.

To pinpoint the ignition and extinction points and locate the limiting boundaries of the multiple steady state region, one needs to search for minimum and maximum values of R_{load} versus T^S. Figure 3 shows the multiplicity region of the cathode and anode gas channel temperature versus load resistance for different values of the heat transfer coefficient, α. The shaded areas in Figure 3 show the regions of the cell inlet gas temperatures and the load resistance, within which

TABLE 1. PARAMETER VALUES OF THE MODEL

parameter	value	source
d_A	10^{-4} m	[7]
d_C	0.5×10^{-4} m	[7]
d_E	1.8×10^{-4} m	[7]
L	0.04 m	[4]
B	0.04 m	[7]
$\dot{n}_{air,in}^{cat}$	3.8×10^{-2} mol s^{-1}	[7]
$\dot{n}_{fuel,in}^{an}$	1.39×10^{-3} mol s^{-1}	[7]
H^A	10^{-3} m	[4]
H^C	10^{-3} m	[4]
$T_{air,in}^{cat}$	950 K (nominal value)	
$T_{fuel,in}^{an}$	950 K (nominal value)	
v_{fuel}^{an}	2.88 m s^{-1}	
v_{air}^{cat}	78.98 m s^{-1}	
$(\rho c_p)^s$	10^6 J m^{-3}K^{-1}	[4]
$\Delta_R H$	-241830 J mol^{-1}	[4]
γ^A	5.7×10^7 A m^{-2}	[7]
γ^C	7×10^9 A m^{-2}	[7]
θ_a^A	2	[7]
θ_c^A	1	[7]
θ_a^C	1.4	[7]
θ_c^C	0.6	[7]
β_1	3.34×10^4 Ω^{-1}m^{-1}	[7]
β_2	1.03×10^4 K	[7]
E^A	140,000 J mol^{-1}	[7]
E^C	160,000 J mol^{-1}	[7]
α	25 W m^{-2}K^{-1} (nominal value)	[4]
Δ_{ano}	5×10^{-5} m	
Δ_{cat}	5×10^{-5} m	
ε_{cat}	5×10^{-1}	[8]
ε_{ano}	5×10^{-1}	[8]
τ_{ano}	3	[8]
τ_{cat}	3	[8]
δ_{ano}	5×10^{-7}	[9]
δ_{cat}	5×10^{-7}	[9]
υ_{H_2}	7.07	[10]
υ_{O_2}	16.6	[10]
υ_{N_2}	17.9	[10]
υ_{H_2O}	12.7	[10]
$y_{O_2,in}$	0.2	[4]
$y_{N_2,in}$	0.8	[4]
$y_{H_2,in}$	0.9	[4]
$y_{H_2O_{in}}$	0.1	[4]

the multiplicity exists, for different values of the heat transfer coefficient (α). As can be seen, the shape of this region is qualitatively similar at different values of the heat transfer coefficient. As the coefficient increases, the multiplicity region shifts towards lower values of the load resistance. This behavior is expected from the fuel cell: as the heat transfer coefficient increases, the rate of heat dissipation increases, and thus to operate the cell at the same steady-state solid temperature, the electrochemical reactions have to release more thermal energy. The higher rate of heat generation by the electrochemical reactions is possible at a higher current, which corresponds to a lower load resistance.

At low gas channels temperatures, there are multiple steady states for the solid temperature, but at high gas channels temperatures, there is a unique steady state.
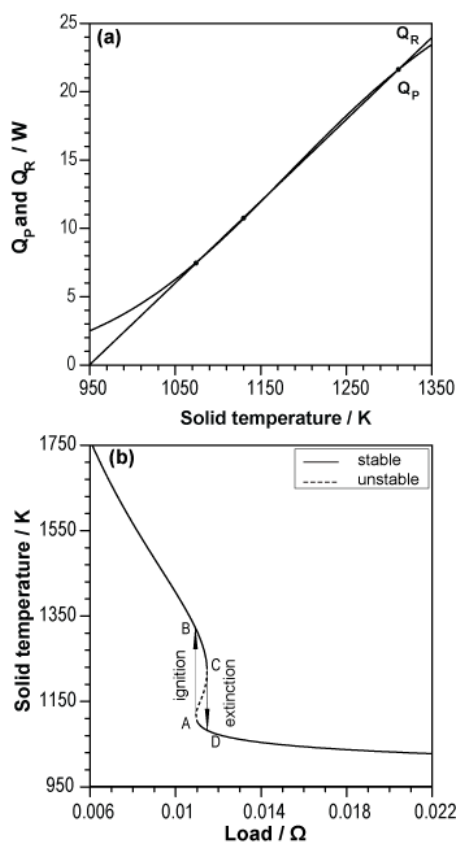

Fig. 3. Multiplicity region for different heat convection coefficients in the constant ohmic load operation.

Fig. 2. Steady state behavior under inlet gas channel temperatures of 950 K: (a) Steady-state heat generation (Q_P) and heat removal (Q_R) versus solid temperature at an external load resistance of 0.0112 Ω; (b) Bifurcation analysis of the model (solid temperature versus load resistance).

Fig. 4. Solid temperature versus load resistance as inlet fuel flow rate varies.

Fig. 5. Solid temperature versus load resistance as inlet air flow rate varies.

We investigated the effect of the inlet fuel and air flow rates on the steady state behavior. Figure 4 is a three dimensional plot of the solid temperature versus the load resistance and the inlet fuel flow rate. As can be seen, the multiplicity region expands as the inlet fuel flow rate increases and the inverse S-shaped curve moves towards lower values of the load resistance.
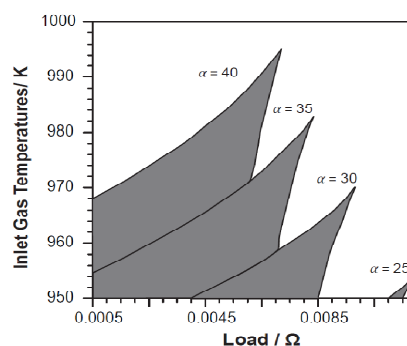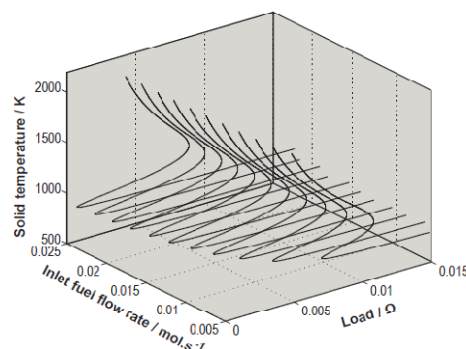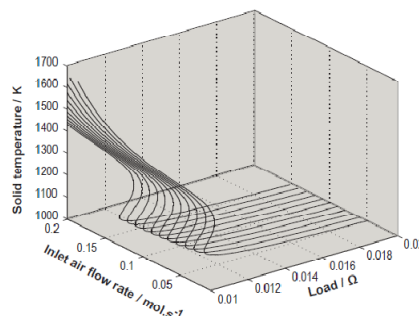
Figure 5 shows the effect of the inlet air flow rate on the solid temperature - load resistance relationship. An increase in the air flow rate moves the inverse S-shaped curve towards the lower values of the load resistance very slightly. One can conclude that the inlet fuel flow rate has more influence on the multiplicity region than the inlet air flow rate does.

B. *Potentiostatic Operation*

The steady state multiplicity was also studied under potentiostatic mode (constant voltage). This mode of operation requires voltage control and is used to characterize a cell. In this case, the cell voltage is the bifurcation parameter. Figure 6 shows the dependence of the multiplicity region on the cell inlet gas temperatures. The values of cell voltage on the boundaries (saddle node bifurcations) were found for different values of the inlet gas channel temperatures to determine the multiple steady state

region. The dependence of multiplicity region on heat convection coefficient is also shown. Similar to the constant ohmic load operation, it can be seen that the multiplicity region shifts towards lower values of the cell voltage. The higher heat convection coefficients means more heat dissipation, and hence lower cell voltages.
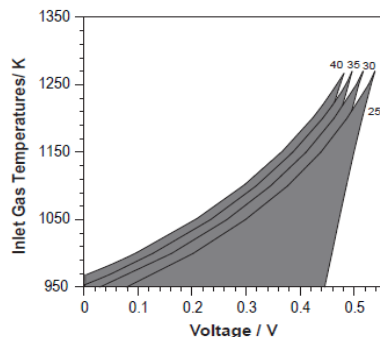

Fig. 6. Multiplicity region for different heat convection coefficient values in the potentiostatic mode.

C. *Galvanostatic Operation*

In the galvanostatic case, the current is kept constant using control. This type of study is used to characterize a cell. In this case, the free parameter is the cell current. The simulation results revealed a unique steady state in all regions. Because of the ACC page limitation, these results are not presented herein.

IV. CONCLUSIONS

The steady state behavior of a SOFC was studied using a detailed lumped model of a planar SOFC. The SOFC system exhibits multiple steady states under certain parameter values. The effects of several operating parameters such as the convection heat transfer coefficients, the inlet gas channel temperatures, and the fuel and air flow rates on the multiplicity behavior of the cell were shown. Intricate behaviors such as steady-state multi-stability and temperature ignition and extinction under constant ohmic load and potentiostatic operations were identified. A unique stable steady state was found in the galvanostatic operation. Furthermore, under identical operating conditions in specific regions; the detailed SOFC model showed a unique steady state, while the lumped simple SOFC model of Mangold et al. [4], which neglected the mass transfer dynamics and heat transfer in the gas channels, exhibited multiple steady states. We also found that the inlet fuel flow rate has more influence on the multiplicity region than the inlet air flow rate does.

NOMENCLATURE

Notation
B= width of cell (m)
C_p= specific heat capacity of the solid (J mol^{-1} K^{-1})
d_A= thickness of anode (m)
d_C= thickness of cathode (m)
d_E= thickness of electrolyte (m)

E^A= activation energy of the anodic reaction (J mol^{-1})
E^C= activation energy of the cathodic reaction (J mol^{-1})
E^0= standard potential (V)
F= faraday constant (A s mol^{-1})
H= height of gas channels (m)
ΔH_R= enthalpy change of the overall reaction (J mol^{-1})
i= current density (A m^{-2})
L= length of cell (m)
$\dot{n}$= molar flow rate (mol s^{-1})
T= temperature (K)
v= velocity (m s^{-1})
y_j= mole fraction of species j

Greek Letters
α = heat transfer coefficient (W m^{-2} K^{-1})
β_1, β_2 = parameters in Eq.8
γ = pre-exponential kinetic factor (A m^{-2})
δ = pore mean radius (m)
Δ = thickness of the diffusion layer (m)
ε = porosity
η = activation overpotential (V)
θ= charge transfer coefficient
υ= diffusion volumes for molecules
ρ = resistivity (Ω m)
ρ^s = density of the solid (kg m^{-3})
τ = tortuosity

Superscripts
A =anode
C=cathode
E=electrolyte
S=solid

References

[1] S. Haile, "Materials for fuel cells," *Materials Today,* vol. 6, pp. 24-29, 2003.
[2] N. Lu, *et al.*, "The modeling of a standalone solid-oxide fuel cell auxiliary power unit," *Journal of Power Sources,* vol. 161, pp. 938-948, 2006.
[3] P. Debenedetti and C. Vayenas, "Steady-state analysis of high temperature fuel cells," *Chemical Engineering Science,* vol. 38, pp. 1817-1829, 1983.
[4] M. Mangold, *et al.*, "Theoretical investigation of steady state multiplicities in solid oxide fuel cells," *Journal of Applied Electrochemistry, vol.36,* pp. 265-275, 2006.
[5] S. A. Hajimolana and M. Soroush, "Dynamics and Control of a Tubular Solid-Oxide Fuel Cell," *Industrial & Engineering Chemistry Research,* vol. 48, p. 7, Jul 2009.
[6] S. Kakac, *et al.*, "A review of numerical modeling of solid oxide fuel cells," *International Journal of Hydrogen Energy,* vol. 32, pp. 761-786, May 2007.
[7] P. Costamagna and K. Honegger, "Modeling of solid oxide heat exchanger integrated stacks and simulation at high fuel utilization," *Journal of the Electrochemical Society,* vol. 145, p. 3995, 1998.
[8] S. Campanari and P. Iora, "Definition and sensitivity analysis of a finite volume SOFC model for a tubular cell geometry," *Journal of Power Sources,* vol. 132, pp. 113-126, 2004.
[9] S. Chan, *et al.*, "A complete polarization model of a solid oxide fuel cell and its sensitivity to the change of cell component thickness," *Journal of Power Sources,* vol. 93, pp. 130-140, 2001.
[10] J. Welty, *et al.*, *Fundamentals of momentum, heat, and mass transfer*: Wiley-India, 2009.
[11] K. Oldham and J. Myland, *Fundamentals of electrochemical science*: Academic Press San Diego, 1993.
[12] R. Bove and S. Ubertini, *Modeling solid oxide fuel cells: methods, procedures and techniques*: Springer Verlag, 2008.